Topological Space-Time Crystal

Yang Peng[1,2,*]
[1]Department of Physics and Astronomy, California State University, Northridge, Northridge, California 91330, USA
[2]Department of Physics, California Institute of Technology, Pasadena, California 91125, USA

(Received 13 January 2022; revised 9 April 2022; accepted 14 April 2022; published 4 May 2022)

We introduce a new class of out-of-equilibrium noninteracting topological phases: the topological space-time crystals. These are time-dependent quantum systems that do not have discrete spatial translation symmetries but instead are invariant under discrete space-time translations. Similar to the Floquet-Bloch systems, the space-time crystals can be described by a frequency-domain-enlarged Hamiltonian, which is used to classify topologically distinct space-time crystals. We show that these space-time crystals can be engineered from conventional crystals with an additional time-dependent drive that behaves like a traveling wave moving across the crystal. Interestingly, we are able to construct 1D and 2D examples of topological space-time crystals based on tight-binding models that involve only one orbital, in contrast to the two-orbital minimal models for any previously discovered static or Floquet topological phases with crystalline structures.

DOI: 10.1103/PhysRevLett.128.186802

Introduction.—Symmetry has been shown to play an important role in topological classification of states of matter. For noninteracting fermionic systems in the presence of discrete spatial translation symmetry (i.e., crystals), the topological phase is characterized by the band structure topology, which is constrained by other coexisting symmetries, including the on-site ones [1–5], and possibly other crystalline symmetries from the crystal's space group [6–14].

Such a symmetry-based topological classification scheme persists even when crystals are driven out of equilibrium, which opens the possibility of engineering desired topological properties with external knobs. As a paradigm, Floquet engineering, i.e., the control of quantum systems by time-periodic external fields, turns out to be extremely powerful. For example, robust electron conducting channels can be brought at the boundary of an otherwise trivial two-dimensional insulator upon a circularly polarized irradiation or an alternating Zeeman field [15–19]. More generally, a complete classification of the Floquet topological insulators and superconductors when considering the on-site symmetries has been obtained in Refs. [20,21], and the classification can be further enriched if more crystalline symmetries are taken into account [22,23].

When exploring the possible topological phases out of equilibrium, besides focusing on the same symmetries as in static situations, space-time symmetries [24,25], which relate different parts of systems at different times, should also be considered, as they arise completely due to the newly added time dimension and have no analog in an equilibrium setup. Indeed, certain space-time symmetries are shown to lead to a different topological classification from the one obtained using purely crystalline symmetries [26–28]. Yet, there are some limitations in these works because the space-time symmetries considered are constrained by requiring the underlying system to be a periodically driven crystal, with separate discrete translation symmetries along spatial and temporal dimensions (which we refer to as the "Floquet-Bloch" scenario).

It has been proposed in Ref. [25] that more space-time symmetries may exist if we remove the above mentioned constraint, and we can have the so-called "space-time crystals," which are characterized by the existence of multiple discrete translation symmetries in the combination of spatial and temporal dimensions. Then one natural question to ask is can we have topologically protected states in such systems? In this Letter, we shall provide a definite answer to this question. An example of a 2D space-time crystal in class A supporting topological protected chiral edge modes is illustrated in Fig. 1.

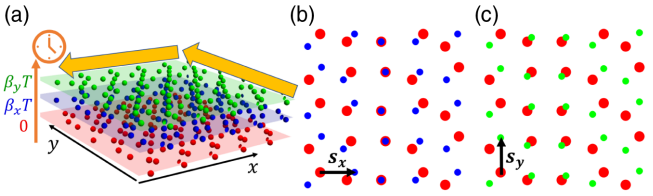

FIG. 1. Illustration of a 2D topological space-time crystal in class A. (a) The vertical orange axis denotes the time coordinate. The 2D noncrystalline lattice system at three different times is shown in three colors. Besides being time periodic with period T, the system is invariant under two additional discrete space-time translations: $(\boldsymbol{s_x}, \beta_x T)$ and $(\boldsymbol{s_y}, \beta_y T)$. The system hosts chiral boundary modes at quasienergy π/T, indicated in yellow arrows. (b),(c) Systems at different times are shown on top of each other (in different colors): $t = 0$ with $t = \beta_x T$, and $t = 0$ with $t = \beta_y T$, respectively. The two spatial translations are also shown.

Space-time crystals.—As first introduced in Ref. [25], the Hamiltonian $H = \xi(\hat{\boldsymbol{p}}) + V(\boldsymbol{r}, t)$ describes a particle moving in $(D+1)$-dimensional space-time, parametrized as $(\boldsymbol{r}, t)$. Here, $\xi(\hat{\boldsymbol{p}})$ is the momentum $(\hat{\boldsymbol{p}})$ dependent kinetic energy, and the potential $V(\boldsymbol{r}, t)$ is assumed to have $(D+1)$ linearly independent discrete space-time translation symmetries along $(\boldsymbol{s}_i, \tau_i)$ for $i = 0, 1, 2, \ldots, D$ as $V(\boldsymbol{r}, t) = V(\boldsymbol{r} + \boldsymbol{s}_i, t + \tau_i)$, which generalizes the familiar Hamiltonian in the Floquet-Bloch case.

Because of the generalized Floquet-Bloch theorem [25], the time-dependent Schrödinger equation $(i\partial_t - H)\psi(\boldsymbol{r}, t) = 0$ admits solutions labeled by the quasimomentum $\boldsymbol{k}$ and quasienergy ω, $\psi_{\boldsymbol{k},\omega}(\boldsymbol{r}, t) = e^{i(\boldsymbol{k}\cdot\boldsymbol{r} - \omega t)} u_{\boldsymbol{k},\omega}(\boldsymbol{r}, t)$, where $u_{\boldsymbol{k},\omega}(\boldsymbol{r}, t)$ has the same space-time translation symmetries as the ones in $V(\boldsymbol{r}, t)$. Similar to the situation in a periodically driven crystal, $\boldsymbol{k}$ and ω are defined up to adding reciprocal vectors of the form $(\boldsymbol{G}_j, \Omega_j)$ with $\boldsymbol{s}_i \cdot \boldsymbol{G}_j - \tau_i \Omega_j = 2\pi\delta_{ij}$, and thus should be restricted in the first (energy-momentum) Brillouin zone (BZ). Moreover, the momentum $\boldsymbol{k}$ and energy ω are not independent and they must solve the following eigenvalue equation:

$$[\xi(\hat{\boldsymbol{p}} + \boldsymbol{k}) + V(\boldsymbol{r}, t) - i\partial_t] u_{\boldsymbol{k},\omega}(\boldsymbol{r}, t) = \omega u_{\boldsymbol{k},\omega}(\boldsymbol{r}, t). \quad (1)$$

To find out the solution at $(\boldsymbol{k}, \omega)$, one can solve the eigenvalues at each $\boldsymbol{k}$ in Eq. (1), and identify solutions that are separated by multiple combinations of reciprocal vectors $(\boldsymbol{G}_j, \Omega_j)$ in energy-momentum space. This can also be seen if we introduce $\tilde{u} = e^{i(\boldsymbol{G}_j\cdot\boldsymbol{r} - \Omega_j t)} u_{\boldsymbol{k},\omega}(\boldsymbol{r}, t)$, then $\tilde{u}$ solves the same type of eigenvalue equation with substitution $\boldsymbol{k} \to \boldsymbol{k} - \boldsymbol{G}_j$, $\omega \to \omega - \Omega_j$, and thus we can denote $\tilde{u} \equiv u_{\boldsymbol{k}-\boldsymbol{G}_j,\omega-\Omega_j}$. Notice that equations similar to Eq. (1) also exist when we simply have Floquet-Bloch systems, in which momentum and energy are separately identified upon addition of multiple reciprocal (to the spatial dimensions) vectors and the driving frequency, respectively. This similarity motivates us to think of band topology in a space-time crystal.

Spectrum.—To generalize the concepts of (Floquet) topological insulators and superconductors to the space-time crystals, we have to focus on systems with an energy gap in the spectrum. However, if there exist more than two nonzero Ω_js in the reciprocal vectors $(\boldsymbol{G}_j, \Omega_j)$, the spectrum will be dense and thus gapless. To see this, one can assume $(\boldsymbol{k}, \omega)$ is a solution, and Ω_1, Ω_2 are two nonzero frequencies in the reciprocal vectors. It implies that all states labeled by $(\boldsymbol{k} + n\boldsymbol{G}_1 + m\boldsymbol{G}_2, \omega + n\Omega_1 + m\Omega_2)$ with $n, m \in \mathbb{Z}$ are also solutions. Since Ω_1 and Ω_2 are incommensurate (otherwise one can redefine reciprocal vectors to make one of them zero), $n\Omega_1 + m\Omega_2$ can be made arbitrarily close to zero with $|n|, |m| \to \infty$, similar to the situation in the quasiperiodically driven case considered in Ref. [29].

Hence, in order to have a "gapped" space-time crystal, we will focus on the particular situations where there only exists one nonzero frequency. In this case, the space-time discrete translation basis vectors can be parametrized as $(\boldsymbol{0}, -T)$, and $(\boldsymbol{s}_j, \beta_j T)$ with $\beta_j \in (-\frac{1}{2}, \frac{1}{2}]$, $j = 1, 2, \ldots, D$. The corresponding reciprocal vectors in energy-momentum space are $(\sum_{j=1}^{D} \beta_j \boldsymbol{G}_j, \Omega)$ with $\Omega = 2\pi/T$, and $(\boldsymbol{G}_j, 0)$ for $j = 1, 2, \ldots, D$. This implies that the potential can be written as

$$V(\boldsymbol{r}, t) = \sum_{n\in\mathbb{Z}} e^{\mathrm{in}(\sum_j \beta_j \boldsymbol{G}_j\cdot\boldsymbol{r} - \Omega t)} V_n(\boldsymbol{r}), \quad (2)$$

where $V_n(\boldsymbol{r}) = V_n(\boldsymbol{r} + \boldsymbol{s}_j)$ is spatially periodic in D dimensions, for all $n \in \mathbb{Z}$ and $j = 1, 2, \ldots, D$. They satisfy $V_n(\boldsymbol{r}) = V_{-n}(\boldsymbol{r})$ because of hermiticity.

Similarly, we can write

$$u_{\boldsymbol{k},\omega}(\boldsymbol{r}, t) = \sum_{n\in\mathbb{Z}} e^{\mathrm{in}(\sum_j \beta_j \boldsymbol{G}_j\cdot\boldsymbol{r} - \Omega t)} u_{n,\boldsymbol{k},\omega}(r), \quad (3)$$

and one can show that the function $u_{n,\boldsymbol{k},\omega}(\boldsymbol{r})$ satisfies

$$[h_0(\boldsymbol{k} + m\delta\boldsymbol{k}) - m\Omega] u_{m,\boldsymbol{k},\omega}(\boldsymbol{r}) + \sum_{n\neq 0} V_n(\boldsymbol{r}) u_{m-n,\boldsymbol{k},\omega}(\boldsymbol{r}) = \omega u_{m,\boldsymbol{k},\omega}(\boldsymbol{r}), \quad (4)$$

where $\delta\boldsymbol{k} = \sum_j \beta_j \boldsymbol{G}_j$, and $h_0(\boldsymbol{k}) = \xi(\hat{\boldsymbol{p}} + \boldsymbol{k}) + V_0(\boldsymbol{r})$ can be interpreted as a Bloch Hamiltonian describing a particle moving in the (spatially) periodic potential $V_0(\boldsymbol{r})$.

Let us denote the eigenstates of $h_0(\boldsymbol{k})$ as $u^j_{\boldsymbol{k}}$ at energy $\epsilon^j_{\boldsymbol{k}}$ (assuming $j = 1, 2, \ldots, d$), and we can expand $u_{m,\boldsymbol{k},\omega} = \sum_j c^j_{m,\boldsymbol{k},\omega} u^j_{\boldsymbol{k}+m\delta\boldsymbol{k}}$. Thus, Eq. (4) can be converted into an eigenvalue equation $\mathcal{H}(\boldsymbol{k})\boldsymbol{C}_{\boldsymbol{k},\omega} = \omega \boldsymbol{C}_{\boldsymbol{k},\omega}$, where we introduced the enlarged Hamiltonian in the frequency domain as

$$\mathcal{H}(\boldsymbol{k}) = \begin{pmatrix} \ddots & & & & \\ & h_0(\boldsymbol{k}-\delta\boldsymbol{k}) + \Omega & h_1^\dagger(\boldsymbol{k}-\delta\boldsymbol{k}) & h_2^\dagger(\boldsymbol{k}-\delta\boldsymbol{k}) & \\ & h_1(\boldsymbol{k}-\delta\boldsymbol{k}) & h_0(\boldsymbol{k}) & h_1^\dagger(\boldsymbol{k}) & \\ & h_2(\boldsymbol{k}-\delta\boldsymbol{k}) & h_1(\boldsymbol{k}) & h_0(\boldsymbol{k}+\delta\boldsymbol{k}) - \Omega & \\ & & & & \ddots \end{pmatrix}. \quad (5)$$

Here, each diagonal block of d dimensions corresponds to a particular frequency sector labeled by m. The column vector $\boldsymbol{C}_{\boldsymbol{k},\omega} = (\ldots, \boldsymbol{c}^T_{-1,\boldsymbol{k},\omega}, \boldsymbol{c}^T_{0,\boldsymbol{k},\omega}, \boldsymbol{c}^T_{1,\boldsymbol{k},\omega}, \ldots)^T$ consists the expansion coefficients of the form $\boldsymbol{c}_{m,\boldsymbol{k},\omega} = (c^1_{m,\boldsymbol{k},\omega}, \ldots, c^d_{m,\boldsymbol{k},\omega})^T$, for all $m \in \mathbb{Z}$. Here, the diagonal blocks are diagonalized with $h_0(\boldsymbol{k}) = \mathrm{diag}(\epsilon^1_{\boldsymbol{k}}, \ldots, \epsilon^d_{\boldsymbol{k}})$ since

eigenstates' basis is used. The off-diagonal blocks $\{h_n(\boldsymbol{k})\}$ are in general nondiagonal and their matrix elements are computed from $[h_n(\boldsymbol{k})]_{ij} = \langle u^i_{\boldsymbol{k}+n\delta\boldsymbol{k}}|V_n|u^j_{\boldsymbol{k}}\rangle$.

It is worth mentioning that $\mathcal{H}(\boldsymbol{k})$ looks very similar to the enlarged Hamiltonian for the Floquet-Bloch problem in the frequency domain formulation [30], except that the off-diagonal blocks no longer couple different Floquet sectors (indexed by m) at the same Bloch momentum $\boldsymbol{k}$ but rather allow mixing of states from different Floquet sectors with momentum differing in multiples of $\delta\boldsymbol{k}$. Thus, we expect these couplings can produce topologically protected energy gaps for space-time crystals.

Space-time crystals from crystals.—The space-time crystals with gapped spectra can be realized from an ordinary crystal (including cold atoms in optical lattices) in equilibrium, described by the Hamiltonian $H_0 = \xi(\hat{\boldsymbol{p}}) + V_0(\boldsymbol{r})$, or simply the Bloch Hamiltonian $h_0(\boldsymbol{k})$. To make the system a space-time crystal, one further generates a traveling wave on the crystal lattices by applying, for example, an acoustic wave (or modulating the optical potential for cold atoms) at angular frequency Ω and wave vector $\delta\boldsymbol{k}$, which produces the term $\sum_{n\neq 0} e^{\mathrm{in}(\delta\boldsymbol{k}\cdot\boldsymbol{r}-\Omega t)}V_n(\boldsymbol{r})$.

When the static crystal with Bloch Hamiltonian $h(\boldsymbol{k})$ is described by a tight-binding model (namely using Wannier functions as a basis), the traveling wave potential generates additional on-site and hopping terms that satisfy the space-time translation symmetries. This can be seen by introducing the Wannier function $|w_{j\boldsymbol{R}}|$ at site $\boldsymbol{R}$ with orbital index j for the crystalline Hamiltonian H_0. The hopping amplitude between neighboring sites (or on-site term for $\boldsymbol{R}' = \boldsymbol{R}$) is given by the matrix elements

$$\langle w_{i\boldsymbol{R}'}|H|w_{j\boldsymbol{R}}\rangle = [\tilde{h}^0(\boldsymbol{R}'-\boldsymbol{R})]_{ij} + \sum_{n\neq 0}[h^n(\boldsymbol{R}',\boldsymbol{R},t)]_{ij},$$

where $[\tilde{h}^0(\boldsymbol{R}'-\boldsymbol{R})]_{ij}$ are the static hopping or on-site terms that only depend on $\boldsymbol{R}'-\boldsymbol{R}$. The time-dependent hopping or on-site terms can be written in the following form [31]:

$$[h^n(\boldsymbol{R}',\boldsymbol{R},t)]_{ij} = e^{\mathrm{in}(\delta\boldsymbol{k}\cdot\boldsymbol{R}'-\Omega t)}[\tilde{h}^n(\boldsymbol{R}'-\boldsymbol{R})]_{ij}, \qquad (6)$$

where $\tilde{h}^n$ is some function depending only on $\boldsymbol{R}'-\boldsymbol{R}$. Thus, we see the time-dependent hopping or on-site terms are invariant if we transform $\boldsymbol{R}'$, $\boldsymbol{R}$, and t according to the space-time translations.

As shown in the Supplemental Material [31], the enlarged Hamiltonian introduced in Eq. (5) can also be derived using the Wannier functions. The tight-binding parameters $[\tilde{h}^n(\boldsymbol{R}'-\boldsymbol{R})]_{ij}$ are related to $\mathcal{H}(\boldsymbol{k})$ through

$$h_n(\boldsymbol{k}) = \sum_{\boldsymbol{R}} e^{-i\boldsymbol{k}\cdot\boldsymbol{R}}\tilde{h}^n(\boldsymbol{R}), \qquad (n\geq 0). \qquad (7)$$

Topological classification.—The topological classification of the space-time crystals now boils down to the classification of the enlarged Hamiltonian $\mathcal{H}(\boldsymbol{k})$ at a particular energy gap, given a set of symmetries.

Let $\mathcal{H}(\boldsymbol{k})$ be in one of the Altland-Zirnbauer (AZ) symmetry classes [1–5], which are determined by the presence or absence of the time-reversal, particle-hole, and chiral symmetries, defined according to $\hat{\mathcal{T}}\mathcal{H}(\boldsymbol{k})\hat{\mathcal{T}}^{-1} = \mathcal{H}(\boldsymbol{k}_*-\boldsymbol{k})$, $\hat{\mathcal{C}}\mathcal{H}(\boldsymbol{k})\hat{\mathcal{C}}^{-1} = -\mathcal{H}(\boldsymbol{k}_*-\boldsymbol{k})$, and $\hat{\mathcal{S}}\mathcal{H}(\boldsymbol{k})\hat{\mathcal{S}}^{-1} = -\mathcal{H}(\boldsymbol{k})$, respectively. Here, $\hat{\mathcal{T}}$ and $\hat{\mathcal{C}}$ are antiunitary operators, while $\hat{\mathcal{S}}$ is unitary. Note that we also generalized the definitions by allowing the time-reversal invariant momentum to be different from zero and located at $\boldsymbol{k}_*$. In other words, this means that under antilinear operation, the momentum is reflected about $\boldsymbol{k}_*/2$ rather than zero. Thus, the classification of topological states at a given energy gap depends on the dimension of $\boldsymbol{k}$ and the AZ symmetry class of $\mathcal{H}(\boldsymbol{k})$, as in the case of topological insulators and superconductors. In principle, one can also consider other spatial symmetries instead of on-site symmetries considered above, which will enrich the topological classification.

We are particularly interested in the topologically protected boundary modes at $\omega = \Omega/2 \bmod \Omega$ with open boundary conditions, which indicates a nontrivial out-of-equilibrium topological state that has no analog in the equilibrium scenario [32,33]. In terms of the enlarged Hamiltonian, this often requires coupling between neighboring diagonal sectors in $\mathcal{H}(\boldsymbol{k})$.

For simplicity, let us consider the harmonic driving protocols when $h_n(\boldsymbol{k})$ vanishes for $|n|\geq 2$. Moreover, let us assume that the driving term $h_1(\boldsymbol{k})$ is small and there are energy overlaps only between neighboring Floquet sectors along the diagonal in $\mathcal{H}(\boldsymbol{k})$, i.e., $h_0(\boldsymbol{k}) \simeq h_0(\boldsymbol{k}+\delta\boldsymbol{k}) - \Omega \simeq -\Omega/2$ for some $\boldsymbol{k}$. With these assumptions, one can write $\mathcal{H}(\boldsymbol{k}) \simeq \mathcal{H}_{\mathrm{eff}}(\boldsymbol{k}) - \rho_0\Omega/2$ for the low energy physics around $-\Omega/2$, where ρ_0 is the two-by-two identity matrix. The topological classification at the energy gap $-\Omega/2$ is then determined by the effective Hamiltonian

$$\mathcal{H}_{\mathrm{eff}}(\boldsymbol{k}) = \begin{pmatrix} h_0(\boldsymbol{k}) & h_1^\dagger(\boldsymbol{k}) \\ h_1(\boldsymbol{k}) & h_0(\boldsymbol{k}+\delta\boldsymbol{k}) \end{pmatrix} + \frac{\Omega}{2}\rho_z, \qquad (8)$$

where we introduced the Pauli matrices $\rho_{x,y,z}$ corresponding to the Floquet sectors.

1D model in class D.—It is known that 1D crystals in class D with a particle-hole symmetry $\hat{\mathcal{C}}^2 = 1$ have $\mathbb{Z}_2$ topological invariants and can support Majorana boundary modes. In fact, 1D space-time crystals in class D can also be topological at quasienergy $\Omega/2$, where nontrivial boundary modes exist. Such a model can be constructed using the harmonic driving protocol described by the effective Hamiltonian $\mathcal{H}_{\mathrm{eff}}(\boldsymbol{k})$ in Eq. (8). Consider $h_0(k) = -2w\cos(ka)$ and $h_1(k) = \Delta\cos(ka+\delta ka/2)$, it is obvious that we have a particle-hole symmetry realized via $\rho_x\mathcal{H}_{\mathrm{eff}}(k)\rho_x = -\mathcal{H}_{\mathrm{eff}}(\pi-\delta k-k)^*$. As shown in the

Supplemental Material [31], this symmetry also exists for the full $\mathcal{H}(k)$.

We first take $\delta ka = \pm\pi$; then $\mathcal{H}_{\text{eff}}(k)$ takes the familiar form of the Hamiltonian for the Kitaev chain [34], a toy model for the topological superconductor that hosts boundary Majorana modes in an open chain for $4w \gtrsim \Omega$. On the other hand, even if δka deviates from $\pm\pi$, the particle-hole symmetry persists, and thus the boundary modes should not disappear as along as the bulk gap does not close.

Written in real space, the system is described by a one-orbital tight-binding model along x direction with lattice spacing a:

$$H_{1\text{D}} = \sum_x \{[-w + f(x,t)]\psi_x^\dagger \psi_{x+a} + \text{H.c.}\}, \tag{9}$$

where we have in the hopping parameter a space-time translation invariant modulation $f(x,t) = \Delta\cos\{\delta kx - \Omega t + [(\delta ka)/2]\}$, which satisfies $f(x,t) = f(x, t - 2\pi/\Omega) = f(x + a, t + \delta ka/\Omega)$. The second-quantized operator $\psi_x^\dagger$ (ψ_x) creates (annihilates) an electron on site x.

The numerical results for the band structure of the full enlarged Hamiltonian $\mathcal{H}(k)$ (truncated up to $\pm N_{\text{max}}$ Floquet sector) are shown in Figs. 2(a) and 2(b) for $\delta ka/\pi = 1$ and 0.8, respectively. With an open boundary condition, the system loses its space-time translation symmetry and becomes a Floquet noncrystalline chain. The spectra for such systems at different δk are plotted in Fig. 2(c), which shows that the Majorana boundary modes at quasienergy $\Omega/2$ persist for a considerable range of δka around π. In Fig. 2(d), the absolute value square of the Majorana wave functions traced over all Floquet sectors are plotted for $\delta ka/\pi = 0.8$.

2D model in class A.—It is known that 2D crystals in class A (no symmetries) have a $\mathbb{Z}$ topological invariant, the Chern number. Let us now construct a model for nontrivial 2D space-time crystals in class A, which has been illustrated in Fig. 1. For example, one can take $h_0(\boldsymbol{k}) = 2w[\cos(k_x a) + \cos(k_y a)]$, and $h_1(\boldsymbol{k}) = \Delta[\cos(k_x a + \delta k_x a/2) + i\cos(k_y a + \delta k_y a/2)]$. Choosing $\delta\boldsymbol{k}a = (\pi, \pi)$, the resulting $\mathcal{H}_{\text{eff}}(k)$ becomes the half-Bernevig-Hughes-Zhang model [35], which can support chiral propagating edge modes at the boundary. Now if one considers $\delta\boldsymbol{k}$ away from (π, π), as long as the bulk band gap does not close, the system should be in the same topological phase.

In real space, this system can be described by the following one-orbital tight-binding model on a square lattice with lattice constant a, whose Hamiltonian can be written as $H = H_0 + H_1$, where

$$H_0 = w\sum_{\boldsymbol{R}} (\psi_{\boldsymbol{R}+a\hat{\boldsymbol{x}}}^\dagger \psi_{\boldsymbol{R}} + \psi_{\boldsymbol{R}+a\hat{\boldsymbol{y}}}^\dagger \psi_{\boldsymbol{R}} + \text{H.c.}) \tag{10}$$

describes the static hopping between neighboring sites, while the second term

$$H_1 = \Delta\sum_{\boldsymbol{R}} [\cos(\delta\boldsymbol{k}\cdot\boldsymbol{R} - \Omega t + \delta k_x/2)(\psi_{\boldsymbol{R}+a\hat{\boldsymbol{x}}}^\dagger \psi_{\boldsymbol{R}} + \text{H.c.}) \times \sin(\delta\boldsymbol{k}\cdot\boldsymbol{R} - \Omega t + \delta k_y/2)(\psi_{\boldsymbol{R}+a\hat{\boldsymbol{y}}}^\dagger \psi_{\boldsymbol{R}} + \text{H.c.})] \tag{11}$$

corresponds to the time-dependent hopping with space-time translation symmetries. Here, $\psi^\dagger$ and ψ denote the creation and annihilation operators.

In Fig. 3(a), we show a two-dimensional band structure of $\mathcal{H}(\boldsymbol{k})$ at $w/\Omega = 0.3$ and $\Delta/\Omega = 0.2$ at $\delta\boldsymbol{k}a/\pi = (0.9, 0.9)$, which is expected to be gapped at energy $\Omega/2$ mod Ω. Assuming open boundary condition along y and periodic boundary condition along x, we lost one of the space-time translation symmetries and the enlarged Hamiltonian will only depend on one of the Bloch momentums, k_x. Diagonalizing it at each k_x, we see the

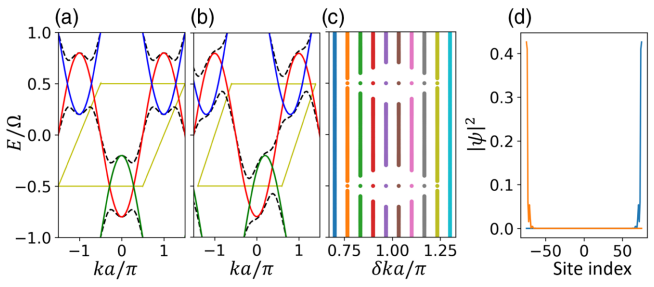

FIG. 2. 1D space-time crystal in class D. (a), (b) show the band structure of $\mathcal{H}(k)$ in black dashed lines for $\delta ka/\pi = 1$ and 0.8, respectively. The red, blue, and green solid lines correspond to the diagonal h_0 in different Floquet sectors. The yellow parallelogram denotes the first energy-momentum BZ. (c) Floquet spectra for an open chain at different δk. (d) Absolute value square of Majorana wave functions traced over Floquet sectors at $\delta ka = 0.8\pi$. The other parameters are $w/\Omega = 0.4$, $\Delta/\Omega = 0.3$, and $N_{\text{max}} = 8$. The open chain contains 150 sites.

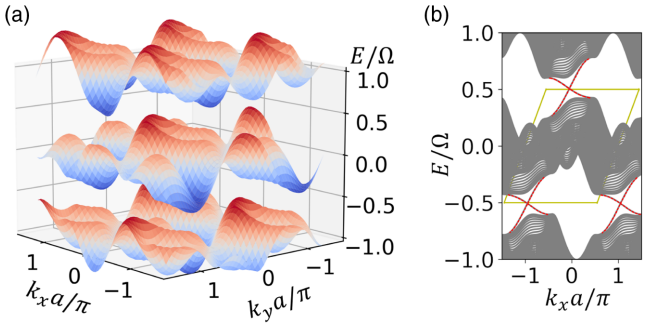

FIG. 3. 2D space-time crystal in class A. (a) Two-dimensional band structure of $\mathcal{H}(\boldsymbol{k})$ for $\delta\boldsymbol{k}a = (0.9\pi, 0.9\pi)$. (b) One-dimensional band structure when periodic boundary condition is assumed only along x. The chiral edge modes inside the bulk gap at $\Omega/2$ are shown with red dotted lines. The energy-momentum BZ is denoted as the yellow parallelogram. The other parameters are $w/\Omega = 0.3$, $\Delta/\Omega = 0.2$, and $N_{\text{max}} = 8$. The number of sites along y is 50 in (b).

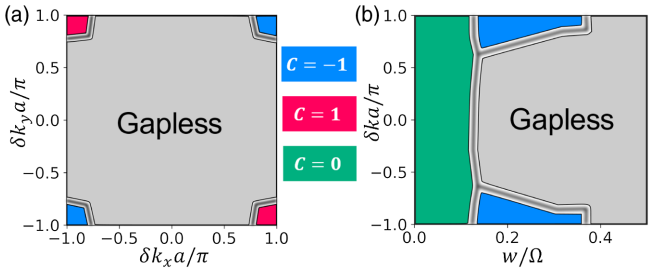

FIG. 4. Phase diagram of 2D space-time crystal in class A. (a) Fixing $w/\Omega = 0.3$, $\Delta/\Omega = 0.2$ while varying δk_x and δk_y, if the system is gapped at quasienergy $\Omega/2$, the topological invariant C is computed. (b) Obtained by fixing $\Delta/\Omega = 0.2$ while varying w and $\delta k \equiv \delta k_x = \delta k_y$.

subgap chiral modes around $\Omega/2$ in Fig. 3(b), as expected. In the Supplemental Material [31], we show that these chiral modes are stable against weak disorder, which is similar to the situation in strong topological insulators.

In Fig. 4(a), the phase diagram as a function of δk_x and δk_y at fixed $w/\Omega = 0.3$ and $\Delta/\Omega = 0.2$ is shown. Apart from a large gapless region, the quasienergy spectrum is found to be gapped at $\Omega/2$ (mod Ω), at which the topological invariant C can be computed by summing over the Chern numbers of all bands below the gap. Note that Cs computed from the enlarged Hamiltonian $\mathcal{H}(\boldsymbol{k})$ at every gapped energy $\Omega/2 + n\Omega$, with $n \in \mathbb{Z}$, are all identical due to the fact that the spectrum is shifted downward by Ω if one performs $\boldsymbol{k} \to \boldsymbol{k} + \delta\boldsymbol{k}$. Numerically, with a finite truncation parameter $N_{\max}$, this means a nonzero Chern number can only be carried by the top and bottommost bands. In Fig. 4(b), the phase diagram as a function of w and $\delta k \equiv \delta k_x = \delta k_y$ at fixed $\Delta/\Omega = 0.2$ is shown.

Conclusion.—In this Letter, we extend the noninteracting topological phases to the scenario of space-time crystals, which are nonequilibrium quantum systems beyond the Floquet paradigm. Particularly, we focused on only a subset of space-time translation symmetries such that the bulk quasienergy spectrum can be gapped. We introduced the enlarged Hamiltonian, similar to the one used in the Floquet case, for the space-time crystal. Thus, the topological classification of the space-time crystal becomes the classification of the enlarged Hamiltonian, a static Bloch-like Hamiltonian. We showed that such space-time crystals can be engineered from conventional crystals with an additional time-dependent drive that behaves like a traveling wave moving across the crystal. We further construct tight-binding models of topological space-time crystals in 1D and 2D to illustrate the general principle.

The topological space-time crystals that support boundary modes at quasienergy $\Omega/2$ mod Ω are intrinsic nonequilibrium topological phases as they have no static analog. More interestingly, the topological nontrivial systems can even be realized in one-orbital tight-binding models, whereas this is impossible for both static and Floquet noninteracting topological phases in which at least two orbitals are required. This would in some sense make topological space-time crystals experimentally even more accessible with a reduced degrees of freedom.

Finally, it is worth mentioning that there are a few directions in which to generalize the results of this work. Although the construction of models in other AZ symmetry classes is straightforward, at least in the case of harmonic driving protocols as we can use the simple effective two-by-two Hamiltonian in Eq. (8), the classification with additional not on-site space-time symmetries from a space-time group [25] will require additional work. Another direction is to remove the restriction to the space-time translation symmetries considered in this work, and this will allow for dense quasienergy spectrum, as in a time-quasiperiodic system [29]. Furthermore, here we only considered noninteracting space-time crystals. The exploration of topological phases that are stable in the presence of electron interactions will be left for future work. On the practical side, it is important to have experimentally feasible ways to detect the boundary modes in topological space-time crystals. One possibility would rely on tunneling into the sample boundary at bias voltage at $\Omega/2$, as proposed for the Floquet-Bloch systems [28,36]. Particularly, the tunneling conductance at the edge will be nonzero due to the spectral weight of the topological modes [37], whereas it is vanishing when the tunneling happens inside the bulk. We numerically calculate this spectral weight for the 1D and 2D models in the Supplemental Material [31].

Y. P. acknowledges support from the startup fund from California State University, Northridge. Y. P. is grateful for the helpful discussions with Gil Refael and Frederik Nathan.

*Corresponding author.
yang.peng@csun.edu

[1] A. P. Schnyder, S. Ryu, A. Furusaki, and A. W. W. Ludwig, Classification of topological insulators and superconductors in three spatial dimensions, Phys. Rev. B **78**, 195125 (2008).
[2] A. Kitaev, Periodic table for topological insulators and superconductors, AIP Conf. Proc. **1134**, 22 (2009).
[3] S. Ryu, A. P. Schnyder, A. Furusaki, and A. W. Ludwig, Topological insulators and superconductors: tenfold way and dimensional hierarchy, New J. Phys. **12**, 065010 (2010).
[4] J. C. Y. Teo and C. L. Kane, Topological defects and gapless modes in insulators and superconductors, Phys. Rev. B **82**, 115120 (2010).
[5] C.-K. Chiu, J. C. Y. Teo, A. P. Schnyder, and S. Ryu, Classification of topological quantum matter with symmetries, Rev. Mod. Phys. **88**, 035005 (2016).
[6] L. Fu, Topological Crystalline Insulators, Phys. Rev. Lett. **106**, 106802 (2011).

[7] C.-K. Chiu, H. Yao, and S. Ryu, Classification of topological insulators and superconductors in the presence of reflection symmetry, Phys. Rev. B **88**, 075142 (2013).
[8] R.-J. Slager, A. Mesaros, and V. Juricić, and J. Zaanen, The space group classification of topological band-insulators, Nat. Phys. **9**, 98 (2013).
[9] K. Shiozaki and M. Sato, Topology of crystalline insulators and superconductors, Phys. Rev. B **90**, 165114 (2014).
[10] Y. Ando and L. Fu, Topological crystalline insulators and topological superconductors: From concepts to materials, Annu. Rev. Condens. Matter Phys. **6**, 361 (2015).
[11] J. Kruthoff, J. de Boer, J. van Wezel, C. L. Kane, and R.-J. Slager, Topological Classification of Crystalline Insulators Through Band Structure Combinatorics, Phys. Rev. X **7**, 041069 (2017).
[12] B. Bradlyn, L. Elcoro, J. Cano, M. Vergniory, Z. Wang, C. Felser, M. I. Aroyo, and B. A. Bernevig, Topological quantum chemistry, Nature (London) **547**, 298 (2017).
[13] Z. Song, T. Zhang, Z. Fang, and C. Fang, Quantitative mappings between symmetry and topology in solids, Nat. Commun. **9**, 1 (2018).
[14] Z. Song, S.-J. Huang, Y. Qi, C. Fang, and M. Hermele, Topological states from topological crystals, Sci. Adv. **5**, eaax2007 (2019).
[15] T. Oka and H. Aoki, Photovoltaic hall effect in graphene, Phys. Rev. B **79**, 081406(R) (2009).
[16] J.-i. Inoue and A. Tanaka, Photoinduced Transition Between Conventional and Topological Insulators in Two-Dimensional Electronic Systems, Phys. Rev. Lett. **105**, 017401 (2010).
[17] T. Kitagawa, T. Oka, A. Brataas, L. Fu, and E. Demler, Transport properties of nonequilibrium systems under the application of light: Photoinduced quantum hall insulators without landau levels, Phys. Rev. B **84**, 235108 (2011).
[18] N. H. Lindner, G. Refael, and V. Galitski, Floquet topological insulator in semiconductor quantum wells, Nat. Phys. **7**, 490 (2011).
[19] N. H. Lindner, D. L. Bergman, G. Refael, and V. Galitski, Topological floquet spectrum in three dimensions via a two-photon resonance, Phys. Rev. B **87**, 235131 (2013).
[20] R. Roy and F. Harper, Periodic table for floquet topological insulators, Phys. Rev. B **96**, 155118 (2017).
[21] S. Yao, Z. Yan, and Z. Wang, Topological invariants of floquet systems: General formulation, special properties, and floquet topological defects, Phys. Rev. B **96**, 195303 (2017).
[22] K. Ladovrechis and I. C. Fulga, Anomalous floquet topological crystalline insulators, Phys. Rev. B **99**, 195426 (2019).
[23] J. Yu, R.-X. Zhang, and Z.-D. Song, Dynamical symmetry indicators for Floquet crystals, Nat. Commun. **12**, 5985 (2021).
[24] T. Morimoto, H. C. Po, and A. Vishwanath, Floquet topological phases protected by time glide symmetry, Phys. Rev. B **95**, 195155 (2017).
[25] S. Xu and C. Wu, Space-Time Crystal and Space-Time Group, Phys. Rev. Lett. **120**, 096401 (2018).
[26] Y. Peng and G. Refael, Floquet Second-Order Topological Insulators from Nonsymmorphic Space-Time Symmetries, Phys. Rev. Lett. **123**, 016806 (2019).
[27] Y. Peng, Floquet higher-order topological insulators and superconductors with space-time symmetries, Phys. Rev. Research **2**, 013124 (2020).
[28] S. Chaudhary, A. Haim, Y. Peng, and G. Refael, Phonon-induced floquet topological phases protected by space-time symmetries, Phys. Rev. Research **2**, 043431 (2020).
[29] Y. Peng and G. Refael, Time-quasiperiodic topological superconductors with majorana multiplexing, Phys. Rev. B **98**, 220509(R) (2018).
[30] A. Gómez-León and G. Platero, Floquet-Bloch Theory and Topology in Periodically Driven Lattices, Phys. Rev. Lett. **110**, 200403 (2013).
[31] See Supplemental Material at http://link.aps.org/supplemental/10.1103/PhysRevLett.128.186802 for the derivation of tight-binding models for space-time crystals, discussions on particle-hole symmetries, signatures of topological edge states in tunneling conductance, and stability of 2D class A space-time crystals against disorder.
[32] M. S. Rudner, N. H. Lindner, E. Berg, and M. Levin, Anomalous Edge States and the Bulk-Edge Correspondence for Periodically Driven Two-Dimensional Systems, Phys. Rev. X **3**, 031005 (2013).
[33] F. Nathan and M. S. Rudner, Topological singularities and the general classification of floquet–bloch systems, New J. Phys. **17**, 125014 (2015).
[34] A. Y. Kitaev, Unpaired majorana fermions in quantum wires, Phys. Usp. **44**, 131 (2001).
[35] B. A. Bernevig, T. L. Hughes, and S.-C. Zhang, Quantum spin hall effect and topological phase transition in hgte quantum wells, Science **314**, 1757 (2006).
[36] C. Peng, A. Haim, T. Karzig, Y. Peng, and G. Refael, Floquet majorana bound states in voltage-biased planar josephson junctions, Phys. Rev. Research **3**, 023108 (2021).
[37] B. M. Fregoso, J. P. Dahlhaus, and J. E. Moore, Dynamics of tunneling into nonequilibrium edge states, Phys. Rev. B **90**, 155127 (2014).